

A wavelet-based multifractal analysis of atmospheric data

Patrick FISCHER

IMB Université Bordeaux 1, CNRS UMR 5251

351, cours de la Libération, 33405 Talence, France

August 30, 2010

Abstract

This study presents a wavelet-based multifractal approach to describe qualitatively and quantitatively the complex temporal patterns of atmospheric data. Monthly time series of geopotential height provided by the National Center for Environmental Protection (NCEP) and daily Northern Annual Modes (NAM) times series provided by Baldwin are used in this study. The results obtained for the stratosphere and the troposphere show that the series display two different multifractal behaviors. For large time scales (several years) the main Hölder exponent for the stratosphere and the troposphere data are negative indicating the absence of correlations. The negative Hölder exponents imply the presence of strong singularities in the time series. For short time scales (from few days to one year), the stratosphere series present long-range correlations with Hölder exponents larger than 0.5, whereas the troposphere data are still uncorrelated. Obviously, in both cases stratosphere and troposphere, the main Hölder exponents increases when the time range decreases.

1 Introduction

Numerical weather predictions based on atmospheric data have little skill beyond a week due to the chaotic nature of the physical data (winds, temperatures, pressures, etc). Many physical phenomena range on various time scales: the extratropical QBO with an average period of 28 months, the El Nino Southern Oscillation with a period of about 4 years or the sunspot cycle of 11 years. Some variations on smaller periods of time are well known, like the annual cycle, but the understanding of all the physical phenomena occurring at various time scales is an up-to-date challenge producing many papers every year on the subject (see for instance [8, 9, 10]). Numerical models for the weather prediction are usually based on models describing the lower layer of the atmosphere, the troposphere, and the stratospheric data are generally regarded as having little influence on surface weather patterns. However, large stratospheric anomalies persisting for several weeks or more, occasionally reach Earth's surface [6, 14, 22]. According to Baldwin and Dunkerton, some large circulation anomalies in the lower stratosphere are related to shifts in the probability distribution of extreme values of the Arctic and North Atlantic Oscillations (AO and NAO), and that these stratospheric signals may be used as a predictor of tropospheric weather regimes.

We propose in this paper the study of stratospheric and tropospheric anomalies from a multifractal point of view. The relevance of fractals to physics and many other fields was pointed out by Mandelbrot [17, 18] who developed the fractal theory. A quantitative theory of fractals provides mathematical concepts and numerical tools for the description of scaling properties. For fractal objects with a recursive hierarchical structure, the knowledge of few steps of refinement is sufficient for the understanding of the global physical phenomenon. But phenomena that appear in nature do not exhibit such a well ordered architecture. This observation motivated the development of the multifractal formalism by Parisi and Frisch [21,

11] in the framework of the turbulence theory. This formalism relates the scale-dependence of the statistical moments of turbulent velocity fluctuations to the multifractal nature of the points at which abrupt local variations of velocities appear.

The wavelet-based multifractal formalism has been introduced in the nineties by Mallat [15, 16], Arneodo [2, 3, 4], Bacry [5] and Muzy [19]. A wavelet transform can focus on localized signal structures with a zooming procedure that progressively reduces the scale parameter. Singularities and irregular structures often correspond to essential information in a signal. The local signal regularity can be described by the decay of the wavelet transform amplitude across scales. Singularities can be detected by following the wavelet transform local maxima at fine scales.

The paper is organized as follows. The theoretical background about the wavelet-based multifractal formalism is recalled in section 2. The data and the numerical results are described and commented in section 3. Conclusion and final remarks are given in section 4.

2 The wavelet-based multifractal formalism

Since all the results presented in the sequel concern only time-series, only the one dimensional wavelet theory is reminded in this part. The generalization to higher dimension is relatively easy and is usually based on tensor products of one dimensional basis functions. We present here a summary of the theory, and a more complete description can be found in [1, 2, 3, 4, 5, 12, 13, 15, 16, 19].

The strength of a singularity of a function is usually defined by an exponent called Hölder exponent. The Hölder exponent $h(t_0)$ of a function s at the point t_0 is defined as the largest

exponent such that there exists a polynomial $P_n(t)$ of order n satisfying:

$$|s(t) - P_n(t - t_0)| \leq C|t - t_0|^{h(t_0)}, \quad (1)$$

for t in a neighborhood of t_0 . The polynomial P_n can be the Taylor expansion of s around t_0 . If $n < h(t_0) < n + 1$ then s is C^n but not C^{n+1} . The exponent h evaluates the regularity of s at the point t_0 . The higher the exponent h , the more regular the function s . It can be interpreted as a local measure of 'burstiness' in the time-series at time t_0 . A wavelet transform can estimate this exponent by ignoring the polynomial P_n . A transient structure or 'burst' is generally wavelet-transformed to a superposition of wavelets with the same centre of mass and wide range of frequencies.

The wavelet transform is a convolution product of a data sequence with the compressed (or dilated) and translated version of a basis function ψ called the wavelet mother. The scaling and translation are performed by two parameters: the scale parameter a dilates or compresses the mother wavelet to various resolutions and the translation parameter b moves the wavelet all along the sequence:

$$WT_s(b, a) = \frac{1}{\sqrt{a}} \int_{-\infty}^{+\infty} s(t) \psi^* \left(\frac{t - b}{a} \right) dt, \quad a \in \mathbb{R}^{+*}, b \in \mathbb{R}. \quad (2)$$

This definition of the wavelet transform leads to an invariant L^2 measure, and thus conserves the energy ($\|s\|_2 = \|WT_s\|_2$).

In order to evaluate the Hölder exponent, we have to choose a wavelet mother with $m > h$ vanishing moments:

$$\int_{-\infty}^{\infty} t^k \psi(t) dt, \quad (3)$$

for $0 \leq k < m$. A wavelet with m vanishing moments is orthogonal to polynomials of degree $m - 1$. Since $h < m$, the polynomial P_n has a degree n at most equal to $m - 1$ and we can then show that:

$$\int_{-\infty}^{+\infty} P_n(t - t_0) \psi^* \left(\frac{t - b}{a} \right) dt = 0. \quad (4)$$

Let us assume that the function s can be written as a Taylor expansion around t_0 :

$$s(t) = P_n(t - t_0) + C|t - t_0|^{h(t_0)} \quad (5)$$

We then obtain for its wavelet transform at t_0 :

$$WT_s(t_0, a) = \frac{1}{\sqrt{a}} \int_{-\infty}^{+\infty} C|t - t_0|^{h(t_0)} \psi^* \left(\frac{t - t_0}{a} \right) dt \quad (6)$$

$$= C|a|^{h(t_0)+\frac{1}{2}} \int_{-\infty}^{+\infty} |t'|^{h(t_0)} \psi(t') dt'. \quad (7)$$

We have the following power law proportionality for the wavelet transform of the singularity of $s(t_0)$:

$$|WT_s(t_0, a)| \sim a^{h(t_0)+\frac{1}{2}} \quad (8)$$

Then, we can evaluate the exponent $h(t_0)$ from a log-log plot of the wavelet transform amplitude versus the scale a .

However, we cannot compute the regularity of a multifractal signal because its singularities are not isolated. But we can still obtain the singularity spectrum of multifractals from the wavelet transform local maxima.

These maxima are located along curves in the plane (b, a) . This method, introduced by Arneodo et al. [3], requires the computation of a global partition function $Z(q, a)$. Let $\{b_i(a)\}_{i \in \mathbb{Z}}$ be the position of all maxima of $|WT_s(b, a)|$ at a fixed scale a . The partition

function $Z(q, a)$ is then defined by:

$$Z(q, a) = \sum_i |WT_s(b_i, a)|^q. \quad (9)$$

We can then assess the asymptotic decay $\tau(q)$ of $Z(q, a)$ at fine scales a for each $q \in \mathbb{R}$:

$$\tau(q) = \liminf_{a \rightarrow 0} \frac{\log Z(q, a)}{\log a}. \quad (10)$$

This last expression can be rewritten as a power law for the partition function $Z(q, a)$:

$$Z(q, a) \sim a^{\tau(q)}. \quad (11)$$

If the exponents $\tau(q)$ define a straight line than the signal is a monofractal, otherwise the signal is called multifractal: the regularity properties of the signal are inhomogeneous, and change with location.

Finding the distribution of singularities in a multifractal signal is necessary for analyzing its properties. The so-called spectrum of singularity $D(h)$ measures the repartition of singularities having different Hölder regularity. The singularity spectrum $D(h)$ gives the proportion of Hölder h type singularities that appear in the signal. A fractal signal has only one type of singularity, and its singularity spectrum is reduced to one point. The singularity spectrum $D(h)$ for any multifractal signal can be obtained from the Legendre transform of the scaling exponent $\tau(q)$ previously defined :

$$D(h) = \min_{q \in \mathbb{R}} \left(q \left(h + \frac{1}{2} \right) - \tau(q) \right). \quad (12)$$

Let us notice that this formula is only valid for functions with a convex singularity spectrum

[16]. In general, the Legendre transform gives only an upper bound of $D(h)$ [12, 13]. For a convex singularity spectrum $D(h)$, its maximum

$$D(h_0) = \max_h D(h) = -\tau(0) \quad (13)$$

is the fractal dimension of the Hölder exponent h_0 .

Remark: When the maximum value of the wavelet transform modulus is very small, the formulation of the partition function given in (9) can diverge for $q < 0$. A way to avoid this problem consists in replacing the value of the wavelet transform modulus at each maximum by the supremum value along the corresponding maxima line at scales smaller than a :

$$Z(q, a) = \sum_{l \in \mathcal{L}(a)} \left(\sup_{(t, a') \in l, a' < a} |WT_s(t, a)| \right)^q, \quad (14)$$

where $\mathcal{L}(a)$ is the set of all maxima lines l satisfying: $l \in \mathcal{L}(a)$, if $\forall a' \leq a, \exists (x, a') \in l$. The properties of this modified partition function are well described in [3].

3 Multifractal analysis of atmospheric time series

Depending on the application, there are various ways of computing the wavelet transform. For the purpose of compression for instance, an orthogonal wavelet transform on dyadic scales are generally used. For the study of fractals like in this present study, continuous wavelet transforms have been found to be efficient [5]. The wavelet mother has also to be chosen according to the application. When the time series do not have any characteristic scales, or when the goal is to identify discontinuities or singularities, a real wavelet mother

has to be chosen. In this work, we use the N successive derivatives of a Gaussian function:

$$\psi(x) = \frac{d^N}{dx^N} e^{-x^2/2} \quad (15)$$

These functions are well localized in both space and frequency, and have N vanishing moments, as required for a multifractal analysis. The computations have been performed with $N = 1, 2, 4, 6, 8, 10$ but only the results for $N = 2$ are discussed in detail in this paper. The results for other values of N are very similar denoting the absence of any polynomial component. Furthermore, the case $N = 2$ is generally used for fractal analysis and corresponds to the so-called Mexican Hat function.

We have applied the wavelet-based multifractal approach to the analysis of two sets of atmospheric data. The first set consists in the monthly averages of the NCEP Daily Global Analyzes data [20]. They correspond to times series of geopotential height from January 1948 to June 2005. A spatial average from 60°N to 90°N is performed at 17 levels, from 10 hPa down to 1000 hPa. Then the annual cycle is removed by subtracting for each month the corresponding mean in order to focus our study onto the anomalies. In such way, we will be able to detect and to describe the singularities present in the signal. Typical stratospheric and tropospheric representations are shown at 100 hPa and 700 hPa in Figures 1 and 2.

The second set of data consists in the Northern Annular Modes (NAM) at 17 levels from the stratosphere down to the surface level from January 1958 to July 2006 provided by Baldwin [7]. At each pressure altitude, the annular mode is the first Empirical Orthogonal Function (EOF) of 90-day low-pass filtered geopotential anomalies north of 20°N . Daily values of the annular mode are calculated for each pressure altitude by projecting daily geopotential anomalies onto the leading EOF patterns. In the stratosphere annular mode values are a measure of the strength of the polar vortex, while the near-surface annular mode is called

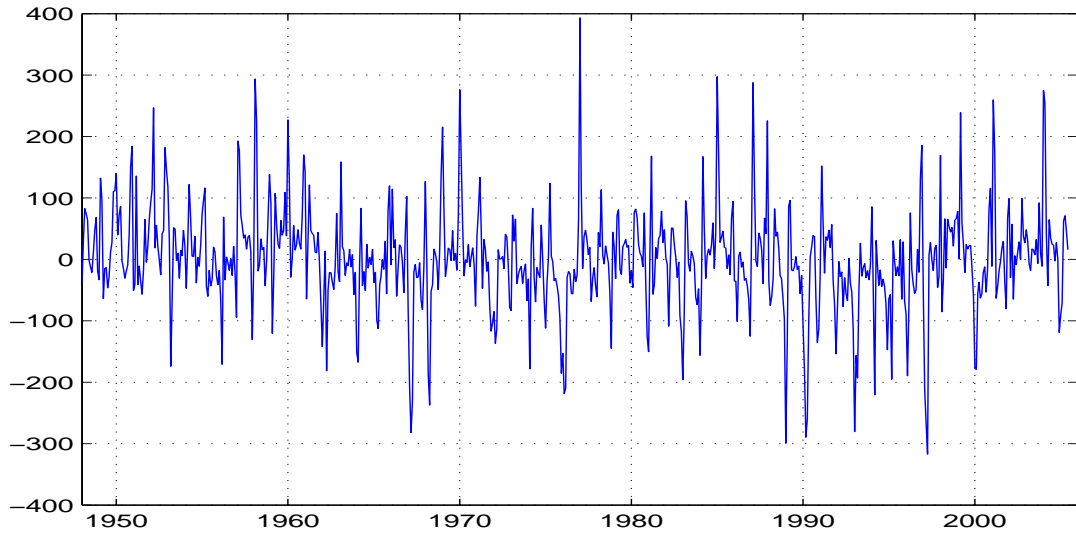


Figure 1: 100 hPa monthly geopotential height anomalies (NCEP) from 1948 to 2005 (spatially averaged from 60°N to 90°N)

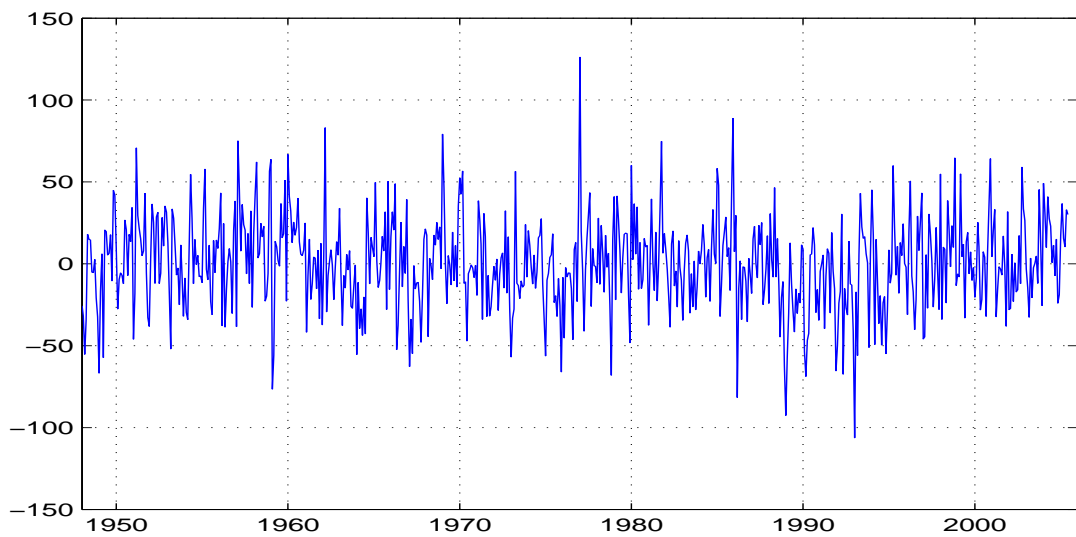


Figure 2: 700 hPa monthly geopotential height anomalies (NCEP) from 1948 to 2005 (spatially averaged from 60°N to 90°N)

the Arctic Oscillation (AO), which is recognized as the North Atlantic Oscillation (NAO) over the Atlantic sector. The NAM signal at 100 hPa and 700 hPa are shown in Figures 3 and 4.

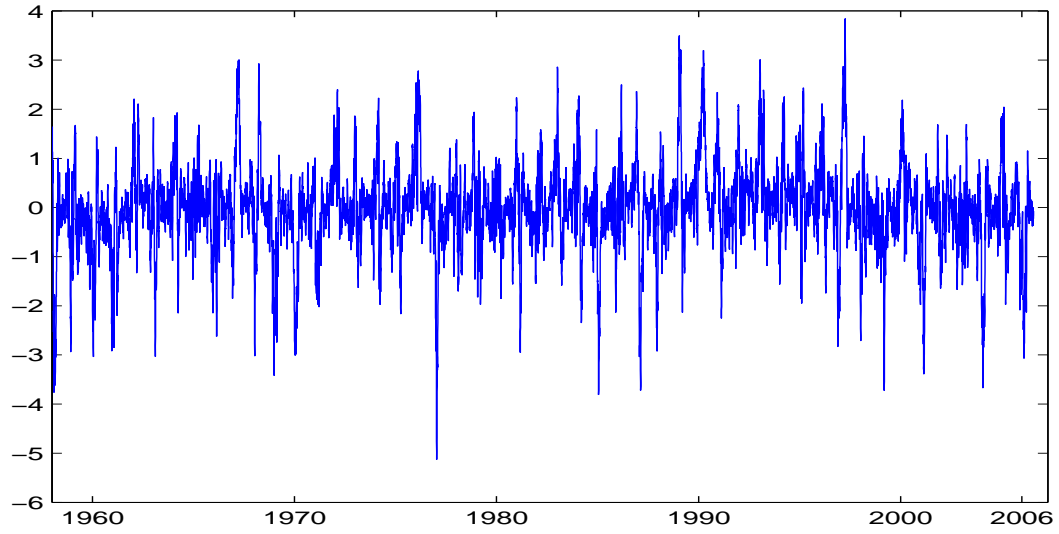


Figure 3: 100 hPa daily anomalies from 1958 to 2006 (NAM index)

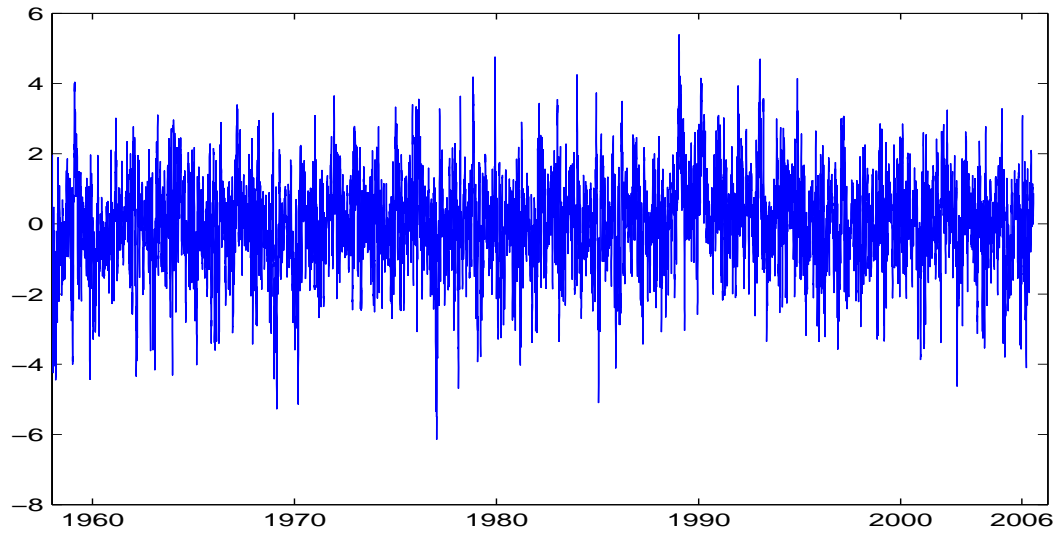


Figure 4: 700 hPa daily anomalies from 1958 to 2006 (NAM index)

3.1 Monthly geopotential height anomalies analysis (NCEP data)

The wavelet decomposition obtained with the Mexican Hat function (second derivative of the Gaussian function) are given in Figures 5 and 6. The wavelet transform consists in

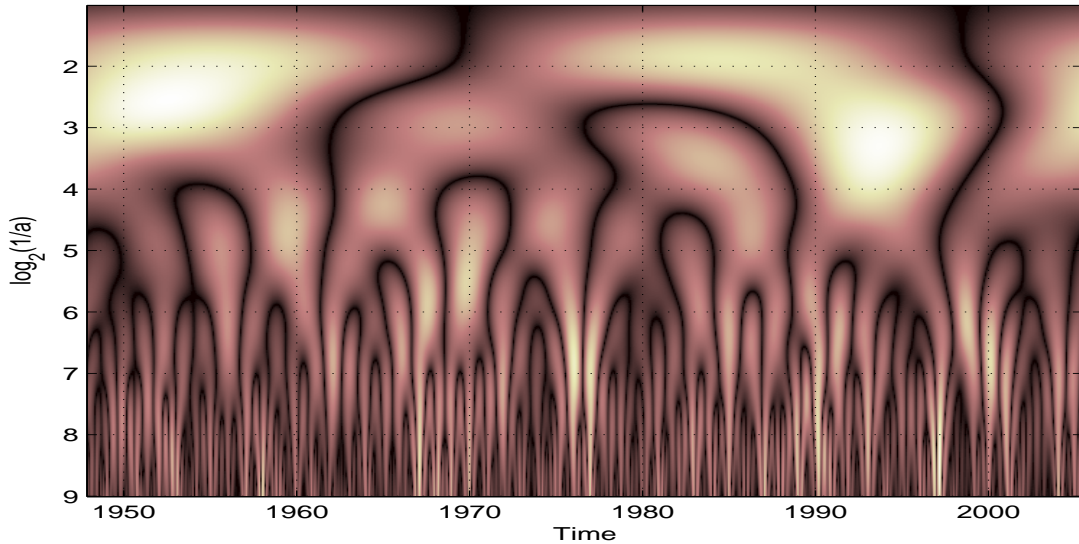


Figure 5: Wavelet transform modulus of the 100 hPa monthly geopotential height anomalies

the calculation of a resemblance index between the signal and the wavelet mother (here the Mexican Hat function). If the signal is similar to itself at different scales, then the wavelet coefficients representation will be also similar at different scales. It can be easily noticed in Figures 5 and 6 that the self-similarity generates a characteristic pattern. This representation is a good demonstration of how well the wavelet transform can reveal the fractal pattern of the atmospheric data. Based only on these representations, we cannot make any significant difference between the stratospheric and the tropospheric signals. But we will see in the sequel by studying the maxima lines of the wavelet transform that these two signals have a different singularity spectrum $D(h)$.

Based on the technical reasons presented in the previous section, the partition function

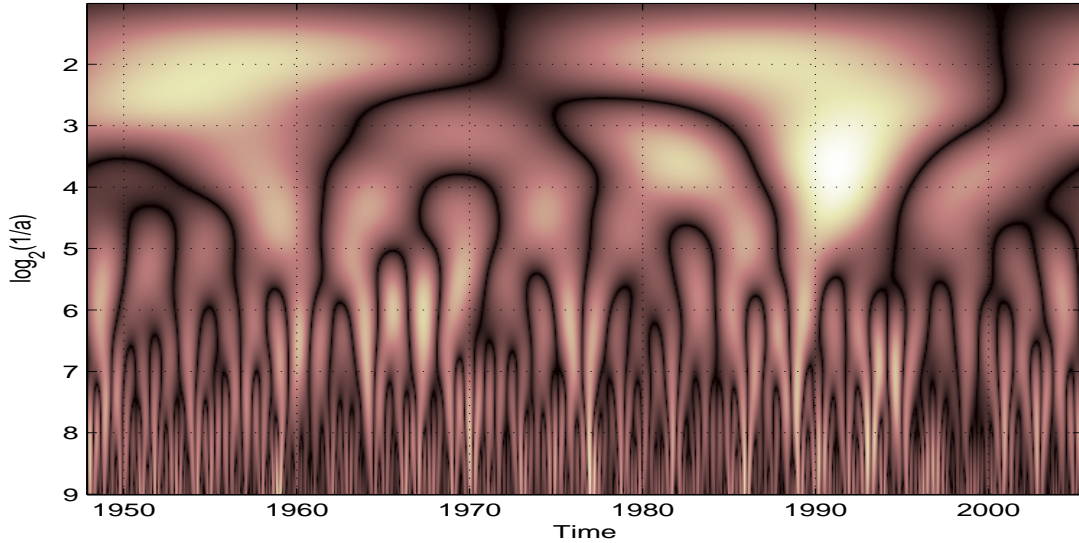


Figure 6: Wavelet transform modulus of the 700 hPa monthly geopotential height anomalies is computed with the formulation given in (14) for q between -20 and 20 with a step size of 0.5.

The first step in the computation of the partition function consists in the detection of the maxima lines of the wavelet transform modulus. The representation of these maxima lines, often called the “skeleton” of the wavelet transform, is given in Figure 7 for the stratospheric signal. For the computation of the partition functions, only the maxima lines of length longer than 1 octave are kept in the summation in order to keep only the significant singularities. The two partition functions are given in Figures 8 and 9. The steps that can be observed for negative values of q are due to the use of the supremum (otherwise, the computation of $Z(q, a)$ would diverge for negative q). We can remark that the slopes for negative q are different for the stratosphere and for the troposphere. Based on this simple remark, we can already predict that the shapes of the corresponding singularity spectra will be also different. We can expect a steeper down slope in the case of the troposphere.

The corresponding singularity spectra are given in Figure 10. The large supports of the

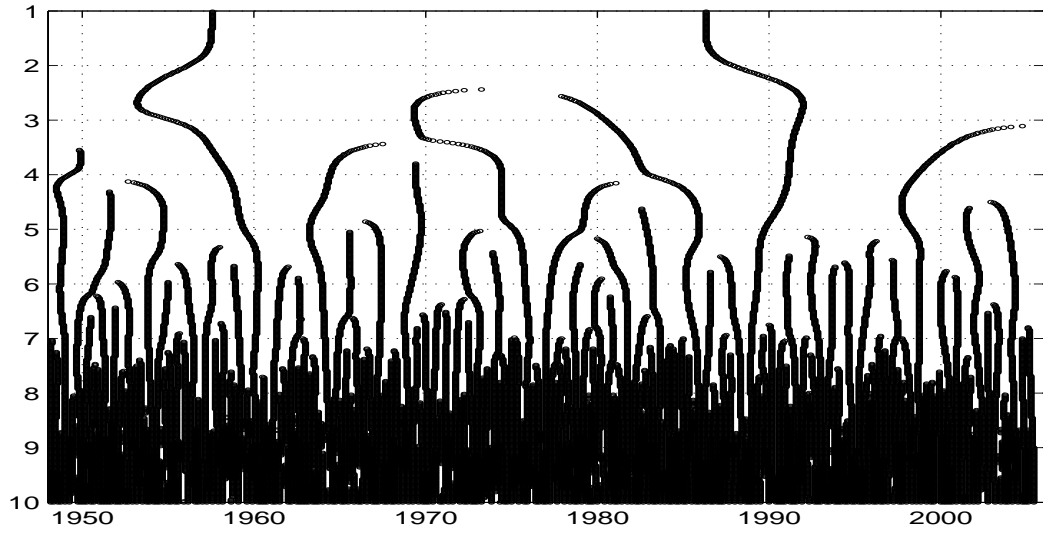


Figure 7: Maxima lines of the modulus of the wavelet transform of the 100 hPa monthly geopotential height signal

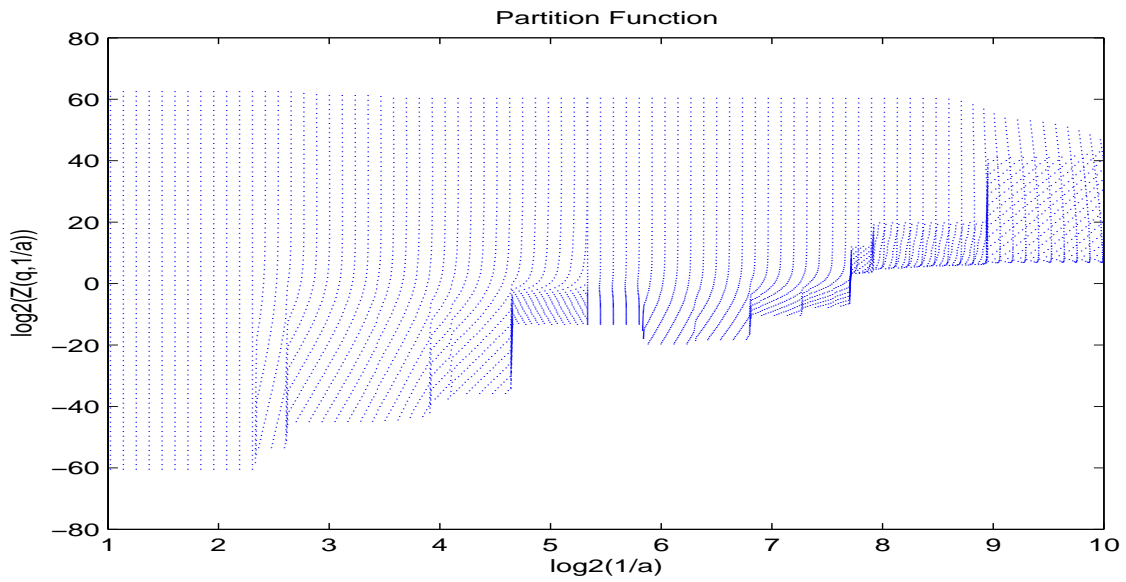


Figure 8: Partition function of the 100 hPa monthly geopotential height signal

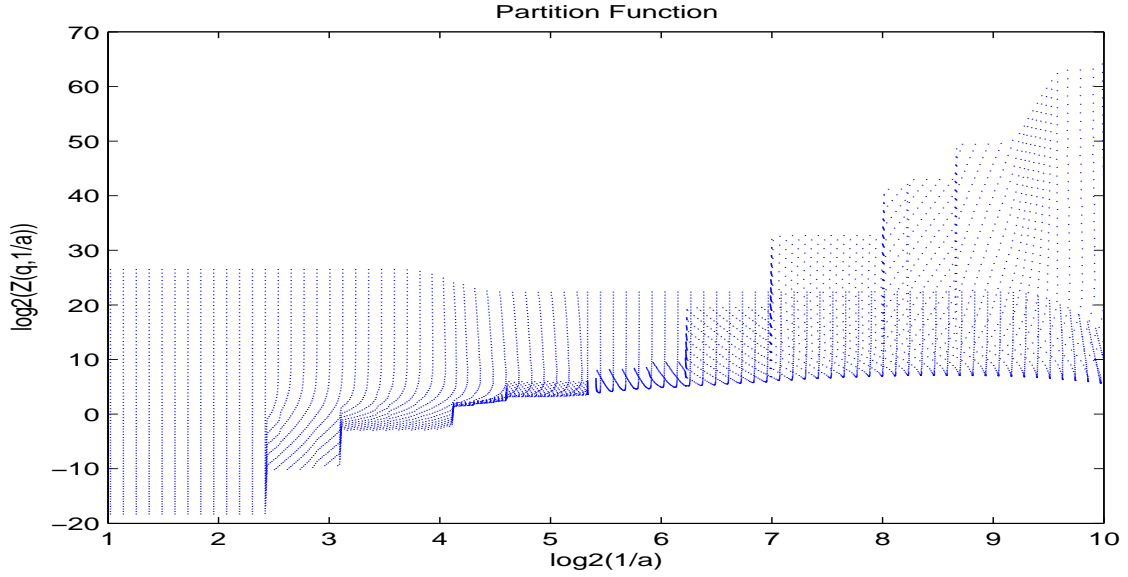


Figure 9: Partition function of the 700 hPa monthly geopotential height signal

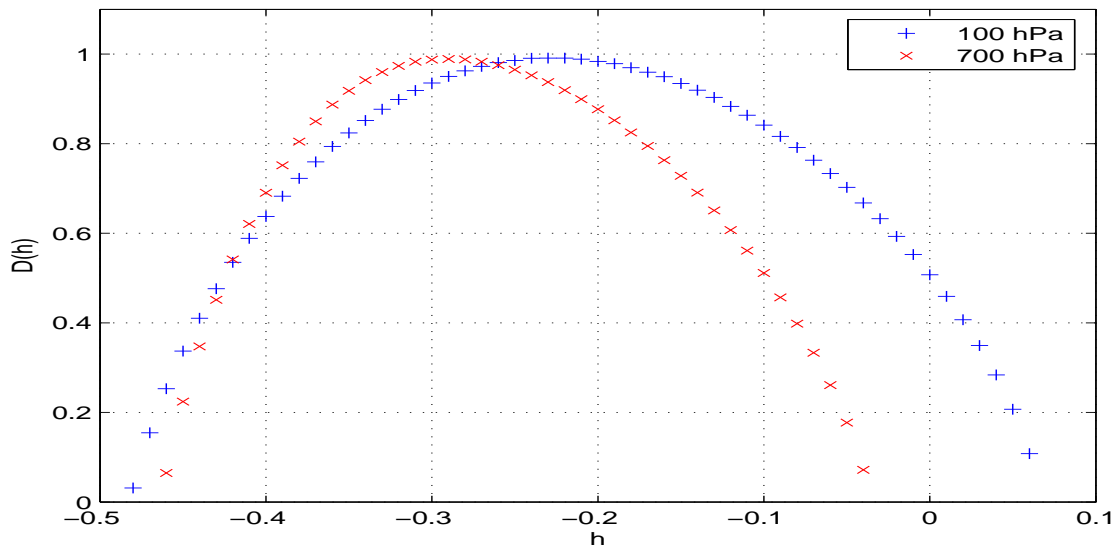


Figure 10: Singularity Spectra of the 100 hPa and 700 hPa monthly geopotential height signals

spectra prove that the signals are multifractal. A quasi-monofractal signal spectrum would lie on very few values, and a real monofractal signal spectrum would reduce to only one point.

As expected, the down slope corresponding to the negative values of q is steeper for the troposphere than for the stratosphere. The maximum of the spectra is obtained around $h = -0.29$ for the stratosphere and between $h = -0.22$ and $h = -0.23$ for the troposphere. We remind here that the smaller is this value the more singular are the singularities in the signal.

So according to this first study, we can conclude that the singularities in the tropospheric signal are more singular than the singularities in the stratospheric signal. We can verify this first conclusion by computing the value of h where the maximum of $D(h)$ is obtained for the 17 levels from 10 hPa down to 1000 hPa. The results are given in Figure 11. We can clearly detect two areas: the first one with h around -0.23 corresponds to the stratosphere and the second one with h around -0.29 corresponds to the troposphere. These results

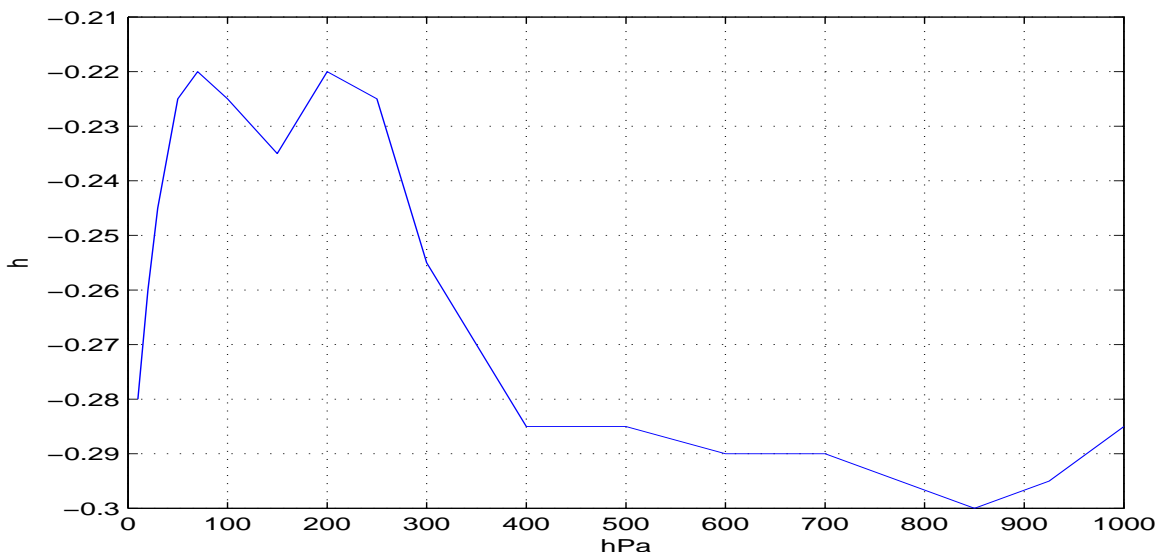


Figure 11: Evolution of h (maximum of $D(h)$) for the 17 levels from 10hPa down to 1000hPa

can be compared to the values h obtained for artificial uncorrelated data. We perform the same computations on signals of random numbers whose elements are uniformly distributed in the interval $(0, 1)$. The value of h found for random signals are around -0.4 . So with $h \sim -0.3$ or $h \sim -0.2$, the signals corresponding to atmospheric data are close to artificial uncorrelated data at these ranges of time periods.

The whole singularity spectra can also give some information to discriminate stratospheric data from tropospheric data. We can show that their supports are also different as can be noticed from Figure 12. The stratospheric signals present broader spectra than the tropospheric signals indicating the presence of singularities over a larger spectrum.

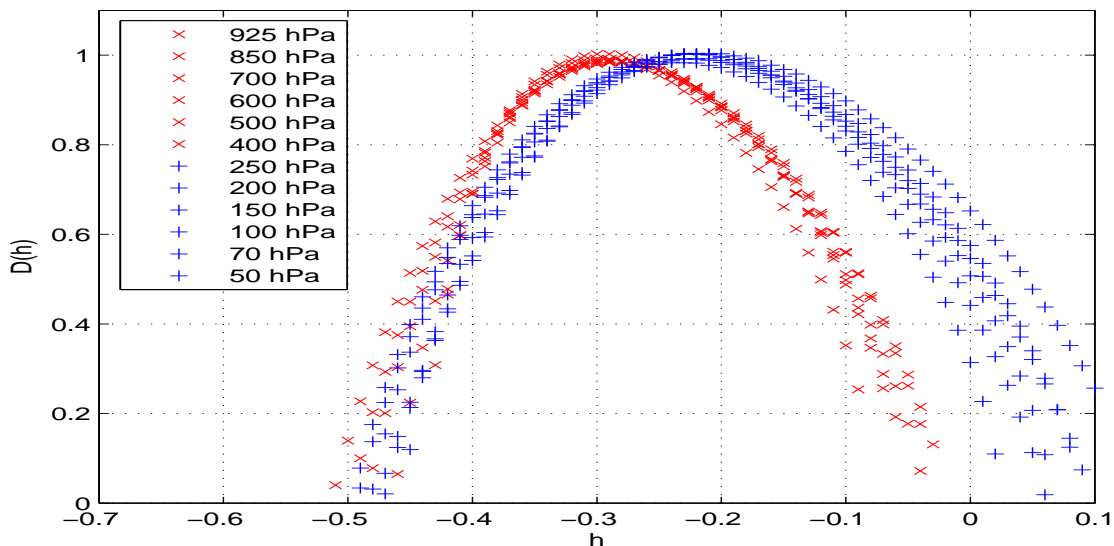


Figure 12: Singularity spectra for few levels of the monthly geopotential height data; stratosphere and troposphere levels are respectively in blue and red

The analysis performed on the monthly averages NCEP Data cannot give any information for periods smaller than a month. In order to get details on finer time periods, we performed the same kind of analysis on the daily NAM index.

3.2 Northern Annular Modes analysis

The NAM data of length 17742 correspond to daily values from January 1958 to July 2006 at 17 levels (from 10 hPa to 1000 hPa). The daily time step size allows to get details on finer time period than the monthly NCEP data. In order to perform some statistics on this large signal, we used 50 sliding windows of various sizes on 8 octaves. The 50 windows are overlapping and regularly spaced. For each window, we performed a continuous wavelet decomposition, and a singularity spectrum computation. We then evaluated the main Hölder exponent h corresponding to the maximum of the singularity spectrum $D(h)$.

The first results shown in Figure 13 correspond to a window of size 1 year for the 17 pressure levels from 10 hPa down to 1000 hPa. The 8 octaves give thus a decomposition from the largest scale (1 year) to the smallest scale (few days). The colormap goes from dark blue for $h = -0.5$ to dark red for $h = 1$. We can easily notice that the main Hölder exponents for the highest stratosphere are bigger than 0.5 which would indicate the presence of long-range dependence. Then the exponents are decreasing with the altitude denoting a more chaotic behavior.

In order to verify the effective presence of correlations in the signal for scales smaller than 1 year, we can replace each window of length 1 year by a shuffled version of the data. By shuffling the series, the correlation is lost but the power law like distribution, if present, remains unchanged. We shuffled our series, and the results are given in Figure 14. The colormap for the shuffled series goes from dark blue for $h = -0.5$ to dark red for $h = -0.25$. The shuffled series are thus completely uncorrelated, and it is then impossible to differentiate the stratosphere data from the troposphere data. These results on shuffled data can be compared to the results obtained for artificial uncorrelated data where random numbers are used instead of the NAM index. The results obtained for the random data are given

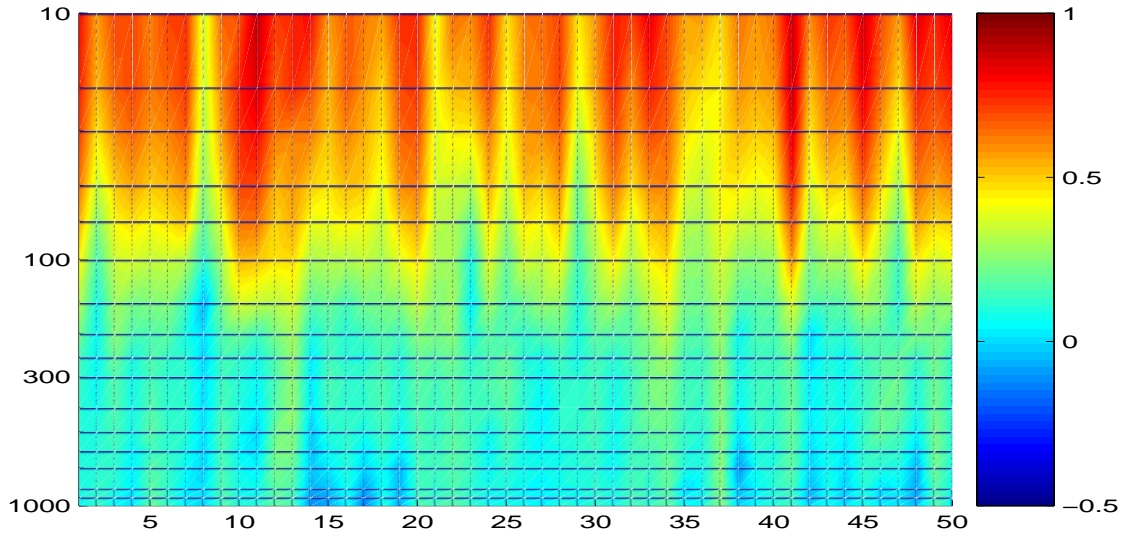


Figure 13: NAM index: Main Hölder exponents h ($\max D(h)$) obtained for the 50 sliding windows (window size: 1 year); X-axis: window number along the signal, Y-axis: the 17 pressure levels from 10 hPa down to 1000hPa, Colormap from blue to red corresponding to Hölder exponents from -0.5 to 1

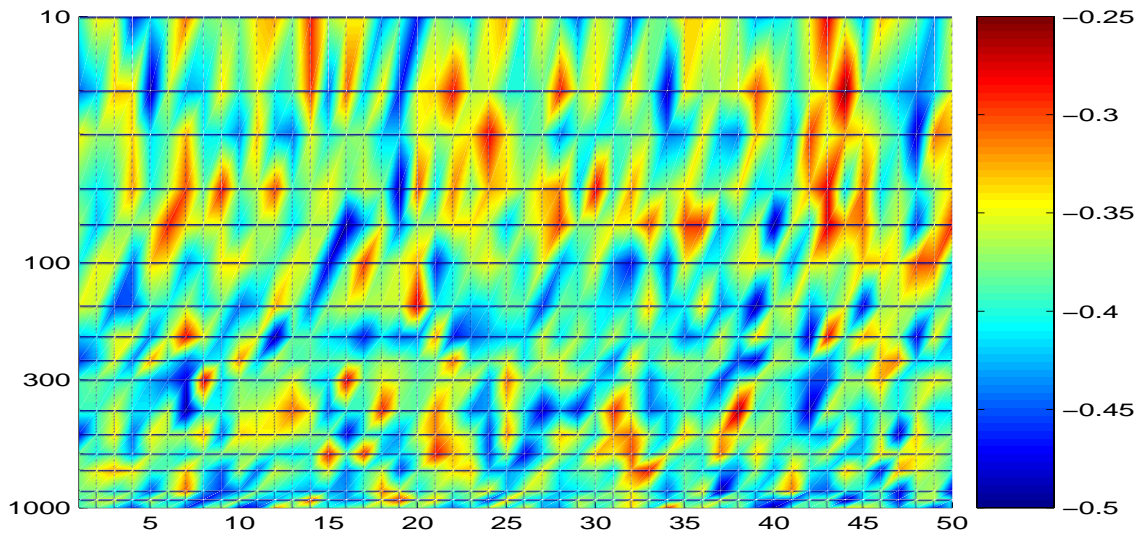


Figure 14: Shuffled NAM data: Main Hölder exponents h ($\max D(h)$) obtained for the 50 sliding windows (window size: 1 year); X-axis: window number along the signal, Y-axis: the 17 pressure levels from 10 hPa down to 1000hPa, Colormap from blue to red corresponding to Hölder exponents from -0.5 to -0.25

in Figure 15. They are very similar to those obtained for the shuffled data. This simple

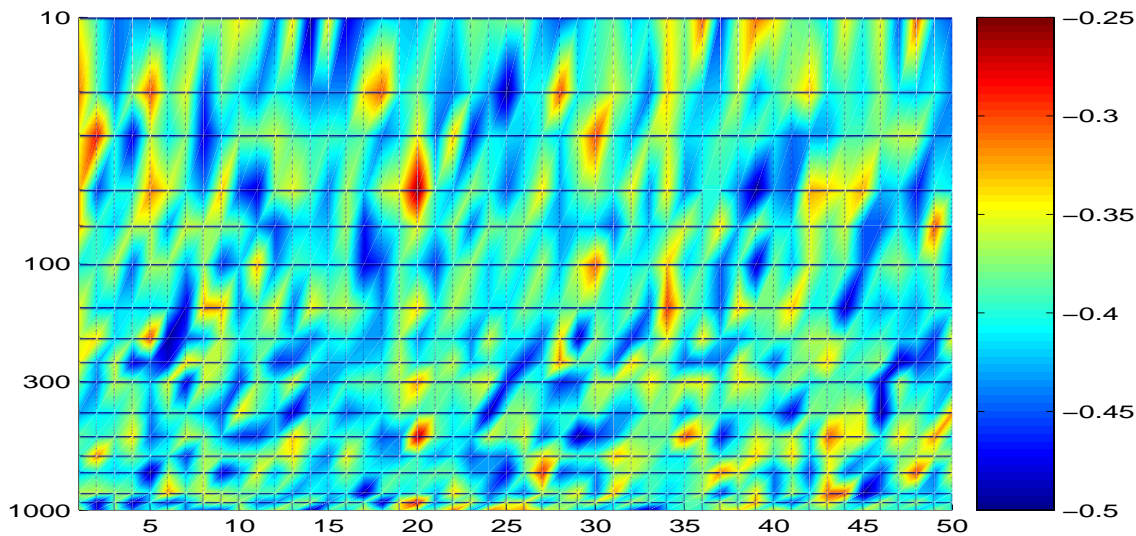


Figure 15: Random data: Main Hölder exponents h ($\max D(h)$) obtained for the 50 sliding windows (window size: 1 year); X-axis: window number along the signal, Y-axis: the 17 pressure levels from 10 hPa down to 1000hPa, Colormap from blue to red corresponding to Hölder exponents from -0.5 to -0.25

test confirms the presence of correlations on time scales between few days and 1 year in the stratosphere layer.

By using a larger window, we are able to verify if this long-range correlation persists to larger periods of time. The results shown in Figure 16 have been obtained with a window of size 5 years on 8 octaves. That means that the largest period is 5 years, and the finest one is few weeks. As can be easily observed, the long-range correlation disappeared in the higher stratosphere, and the non-correlation behavior in the troposphere is stronger. The appearance of negative values for h indicates the presence of strong singularities in the spectra. This trend tends to confirm the results obtained with the monthly NCEP data where negative values had been obtained for h .

In order to validate this trend, another computation with a window of size 25 years has

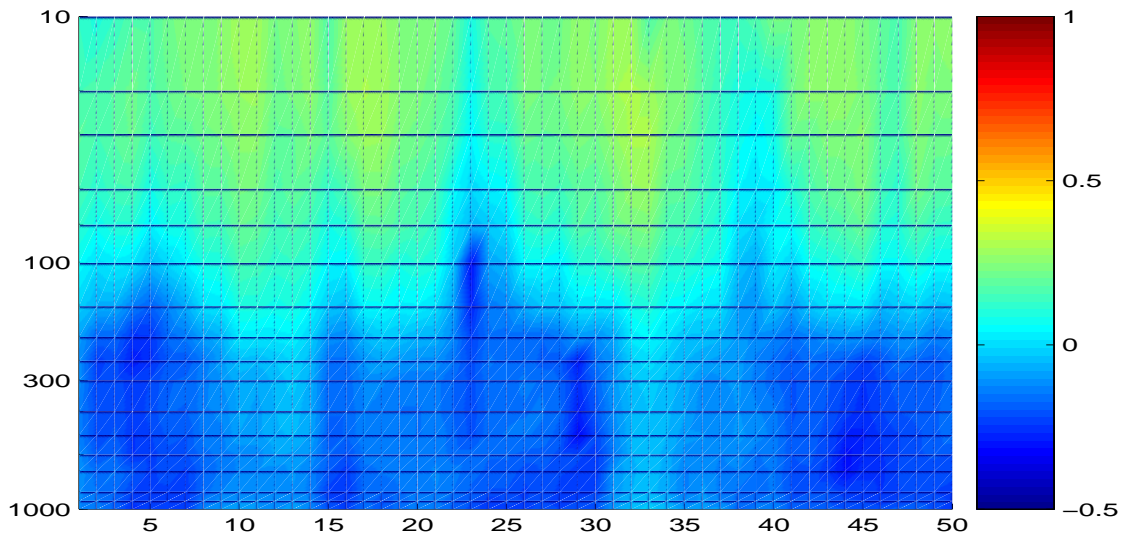


Figure 16: NAM index: Main Hölder exponents h ($\max D(h)$) obtained for the 50 sliding windows (window size: 5 years); X-axis: window number along the signal, Y-axis: the 17 pressure levels from 10 hPa down to 1000hPa, Colormap from blue to red corresponding to Hölder exponents from -0.5 to 1

been performed. The results, given in Figure 17, correspond to a range from 25 years to few months. The trend detected in the two previous experiments is confirmed and we can observe negative values for h at all the altitudes. Even if it's not really clear in Figure 17, the values for h are slightly smaller in the troposphere than in the stratosphere as obtained with the NCEP data computation.

The results with the NAM index presented so far were obtained with decompositions on 8 octaves. While keeping the same octaves number, we can refine the results to describe the fine time periods multifractal behavior. Indeed, we computed the asymptotic decay $\tau(q)$ of the partition function $Z(q, a)$ on the whole large domain, for instance, from 1 year to 5 days for Figure 13. We can cut the domain in the partition function into two parts from 1 year to 45 days, and from 45 days to 5 days, and perform the computation of $\tau(q)$ separately for these two subdomains. The results are given in Figures 18 and 19. The results

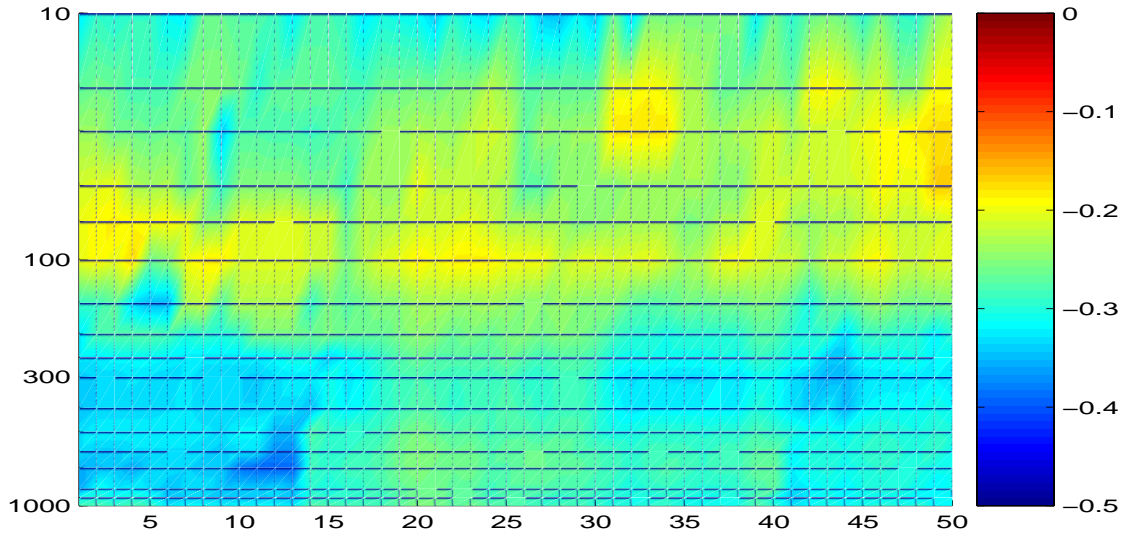


Figure 17: NAM index: Main Hölder exponents h ($\max D(h)$) obtained for the 50 sliding windows (window size: 25 years); X-axis: window number along the signal, Y-axis: the 17 pressure levels from 10 hPa down to 1000hPa, Colormap from blue to red corresponding to Hölder exponents from -0.5 to 0

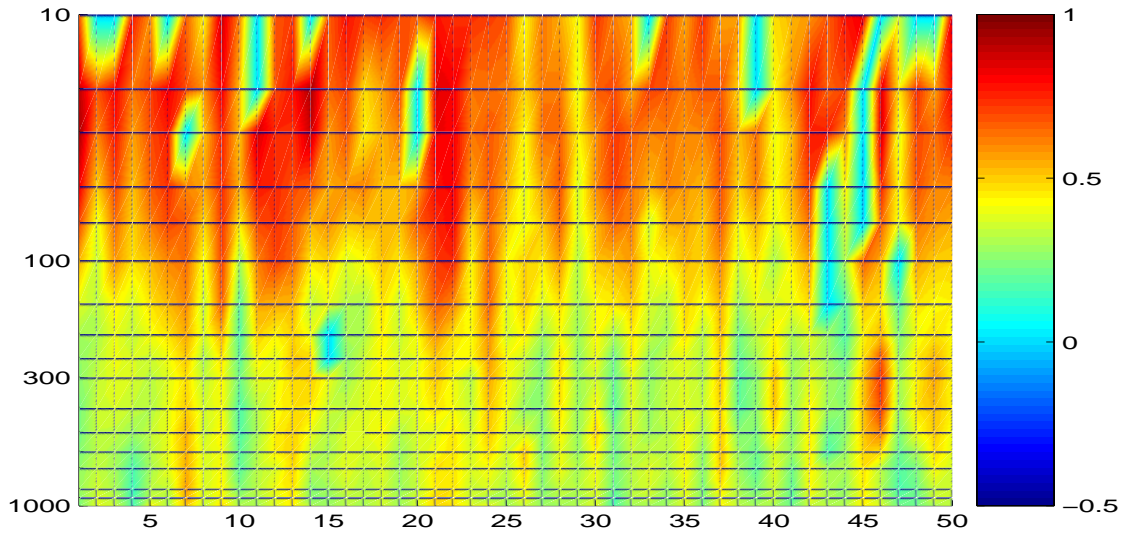


Figure 18: NAM index: Main Hölder exponents h ($\max D(h)$) obtained for the 50 sliding windows (window size: 1 year; partition function domain from 45 days to 5 days); X-axis: window number along the signal, Y-axis: the 17 pressure levels from 10 hPa down to 1000hPa, Colormap from blue to red corresponding to Hölder exponents from -0.5 to 1

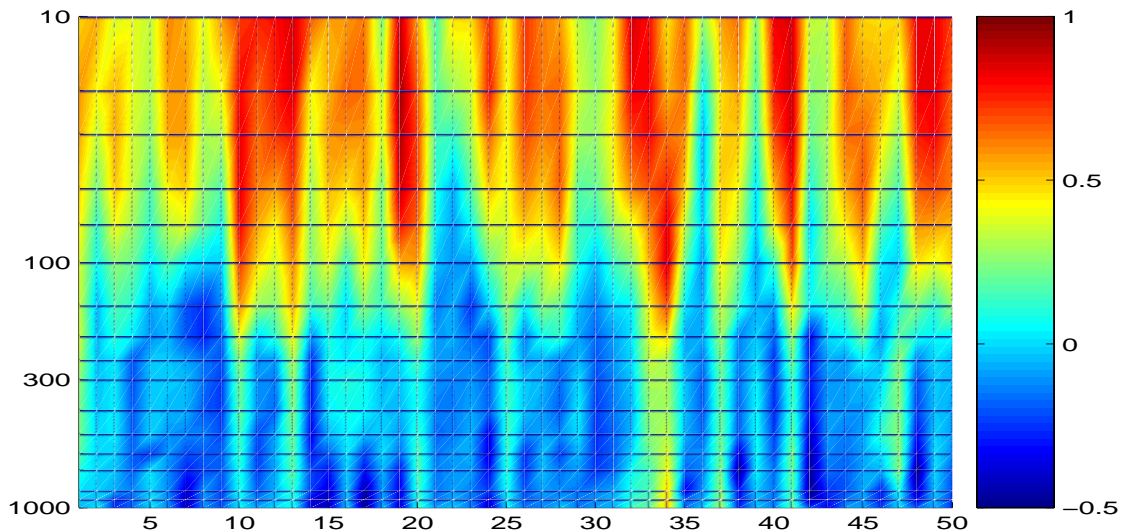


Figure 19: NAM index: Main Hölder exponents h ($\max D(h)$) obtained for the 50 sliding windows (window size: 1 year; partition function domain from 1 year to 45 days); X-axis: window number along the signal, Y-axis: the 17 pressure levels from 10 hPa down to 1000hPa, Colormap from blue to red corresponding to Hölder exponents from -0.5 to 1

are obviously less homogeneous since describing a shorter period of time. We can again notice a difference between the stratosphere and the troposphere in these two figures, the troposphere showing a more singular behavior. At small periods of time, from 45 days to 5 days (Figure 18), the main Hölder exponents for the stratosphere are essentially above 0.5 with only very few small values around 0. At the same range of time, the troposphere data present weaker correlations. This behavior explains the difficulty to make reliable weather predictions in the troposphere on period longer than 5 days. At larger ranges, from 45 days to 1 year (Figure 19), the stratosphere data present large periods of correlation separated by short uncorrelated periods. At these time scales, the troposphere starts to show large periods of uncorrelated data with strong negative values for the main Hölder exponents.

We can detail our study by comparing winter periods to summer periods. We consider periods of length 180 days, first from October to March, and then from April to September.

The results are given in Figure 20 and 21. They don't present any significant difference,

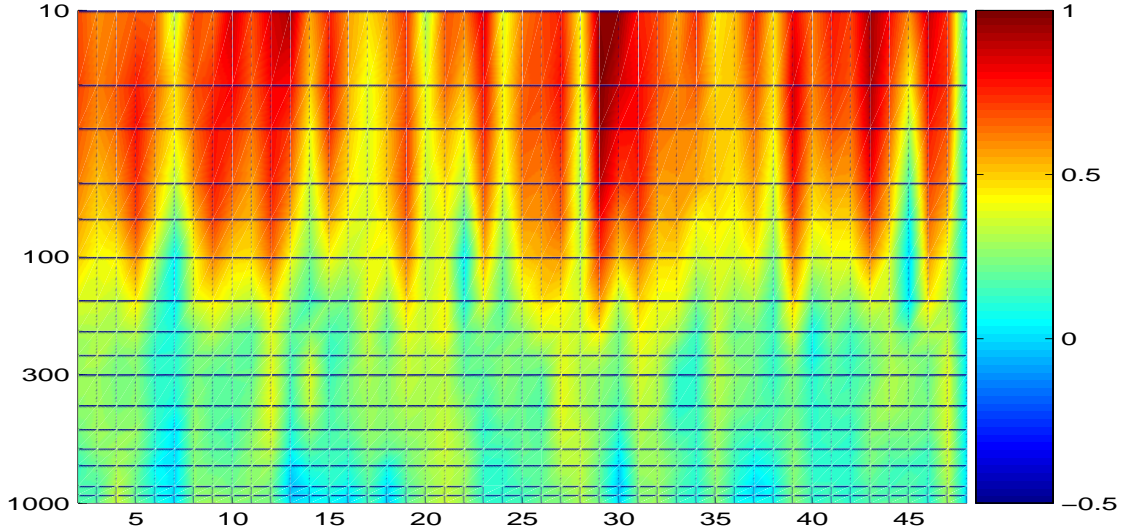


Figure 20: Winter NAM index: Main Hölder exponents h ($\max D(h)$) obtained for the 50 sliding windows (window size: 6 months); X-axis: window number along the signal, Y-axis: the 17 pressure levels from 10 hPa down to 1000hPa, Colormap from blue to red corresponding to Hölder exponents from -0.5 to 1

and we can conclude that the anomalies occurring during the winter months have the same multifractal behavior than the anomalies occurring during the summer months. But on the other hand, the signals are very short and any statistical computations are not really reliable.

Another way to discriminate the atmosphere data from a multifractal point of view consists in studying the support size of the corresponding singularity spectra. So far we only studied the maximum of the spectra, but we can also get some interesting information by studying the support of the spectra. Indeed, the support of a monofractal signal is reduced to only one value since only one Hölder exponent is present in the signal. A signal can be qualified of quasi-monofractal if its singularity spectrum support is very small. A real multifractal signal present a broad singularity spectrum support. If we take into consideration this parameter in the previous computations, and if we plot the the support size in function

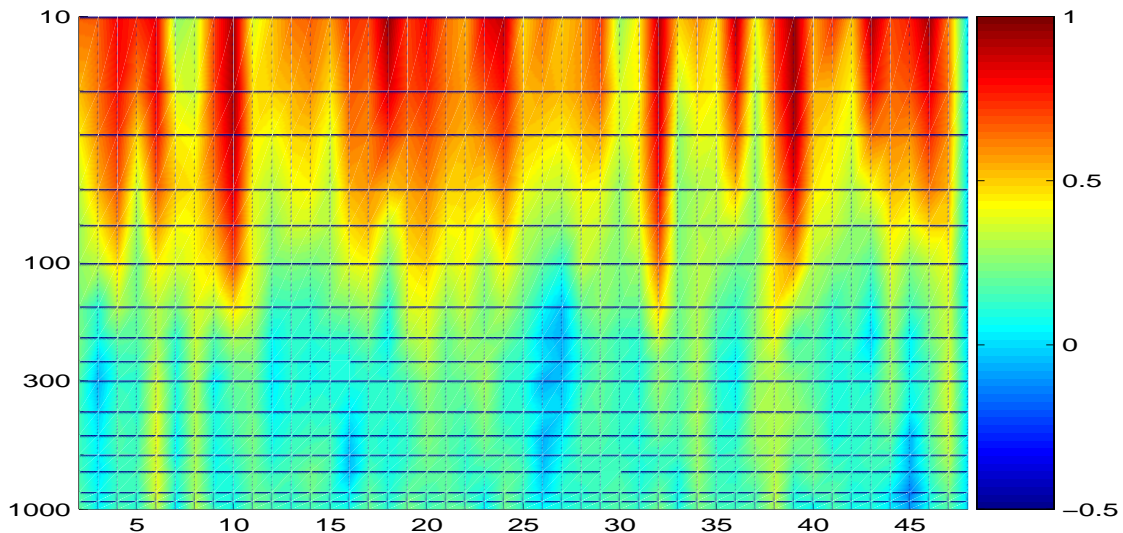


Figure 21: Summer NAM index: Main Hölder exponents h ($\max D(h)$) obtained for the 50 sliding windows (window size: 6 months); X-axis: window number along the signal, Y-axis: the 17 pressure levels from 10 hPa down to 1000hPa, Colormap from blue to red corresponding to Hölder exponents from -0.5 to 1

of the altitude level and of the time, we obtain the results shown in Figure 22. We can again find a different behavior in the stratosphere and the troposphere, the spectrum supports being larger in the stratosphere than in the troposphere. This property can still be observed on larger time range when the size of the window used is of 5 years (fig. 23) or 25 years (fig. 24).

3.2.1 Polynomial component

In order to show the absence of any polynomial component in the signals, we also performed the same computations using wavelet mothers with $N = 1, 2, 4, 6, 8, 10$ vanishing moments. The results were very similar. We report in Figure 25 the singularity spectra obtained for the NAM index (pressure level: 100hPa) with a 25 years window. The values of h obtained for the various wavelet mothers are very close to each other. Then we artificially added a

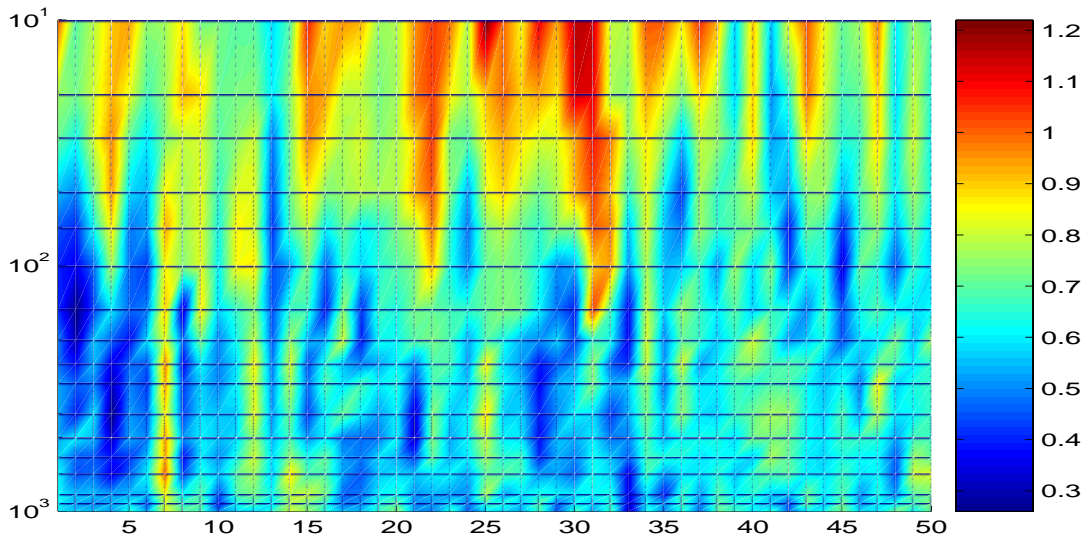


Figure 22: NAM index: Size of the singularity spectrum support obtained for the 50 sliding windows (window size: 1 year); X-axis: window number along the signal, Y-axis: the 17 pressure levels from 10 hPa down to 1000hPa, Colormap from blue to red corresponding to support size from 0.2 to 1.2

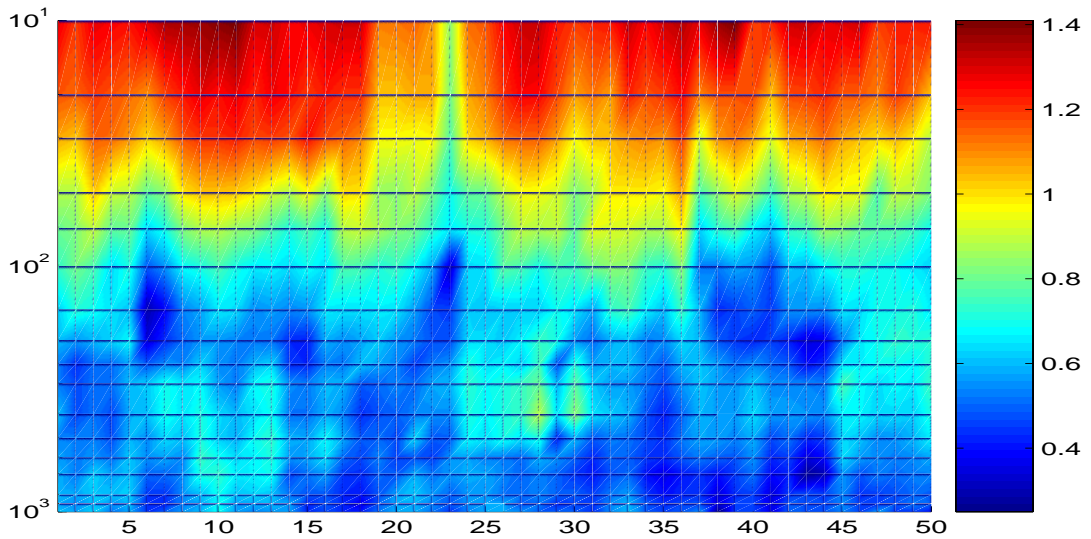


Figure 23: NAM index: Size of the singularity spectrum support obtained for the 50 sliding windows (window size: 5 years); X-axis: window number along the signal, Y-axis: the 17 pressure levels from 10 hPa down to 1000hPa, Colormap from blue to red corresponding to support size from 0.2 to 1.4

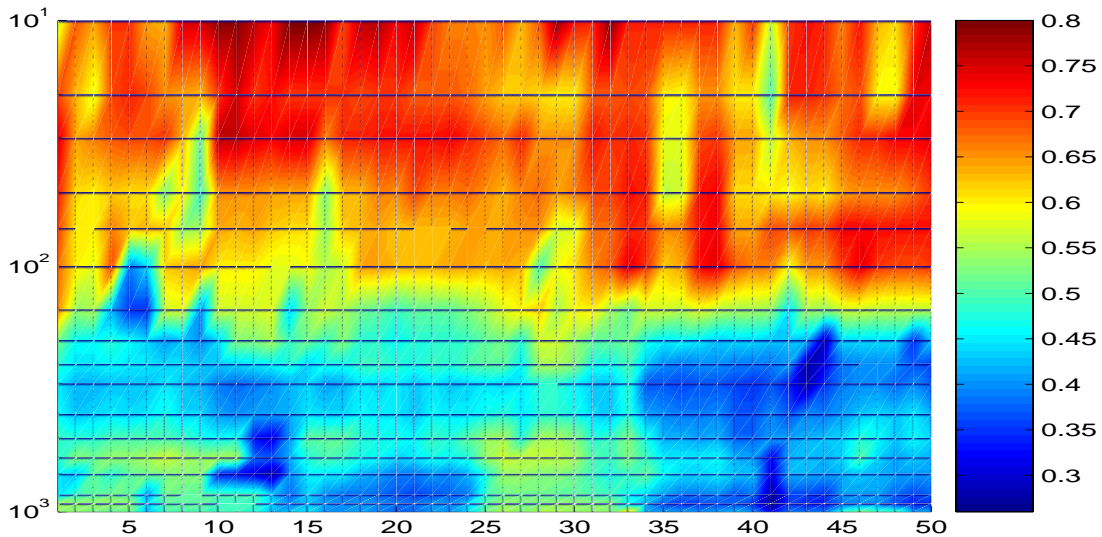


Figure 24: NAM index: Size of the singularity spectrum support obtained for the 50 sliding windows (window size: 25 year); X-axis: window number along the signal, Y-axis: the 17 pressure levels from 10 hPa down to 1000hPa, Colormap from blue to red corresponding to support size from 0.25 to 0.8

quadratic polynomial component to this signal, and we repeated the same computations. It can be easily observed in Figure 26 that the spectra obtained with wavelet mothers with few vanishing moments are modified by the polynomial component. This last test confirms the absence of any polynomial component in the signal, and can be useful in the modelization of atmospheric anomalies.

3.2.2 Red noise comparison

We previously compared the results obtained for the NAM index to the results obtained for a signal composed by random numbers. This kind of random signal is generally used for the creation of white noises. But atmospheric data are usually compared to red noise in the literature. So in order to perform the same kind of comparison, we artificially created a family of red noise signals.

Each discrete time series created depends only on its own immediate past value plus a random

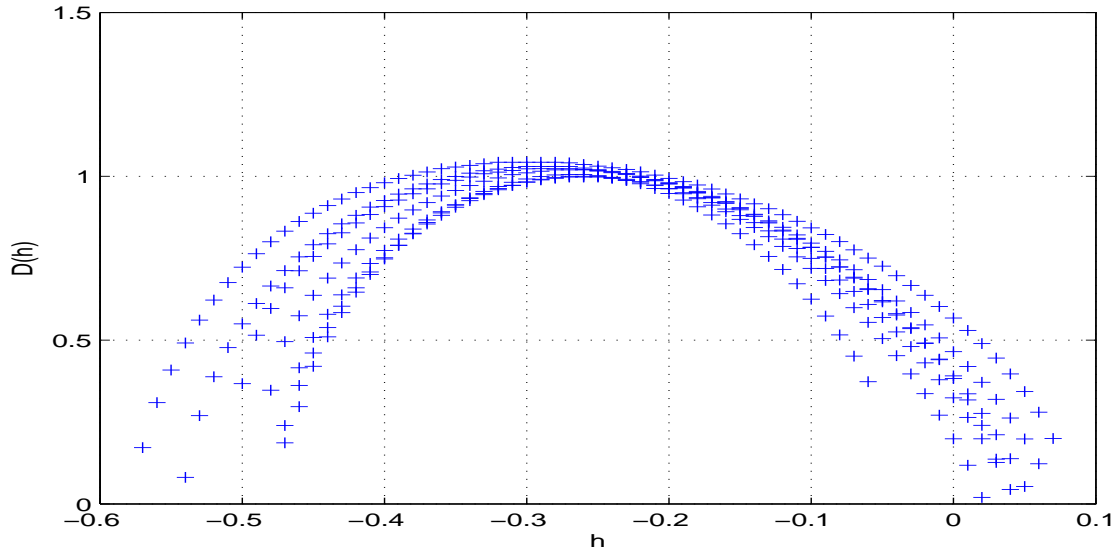


Figure 25: NAM index (100 hPa): Singularity spectra obtained with various derivatives of the Gaussian function as wavelet mother

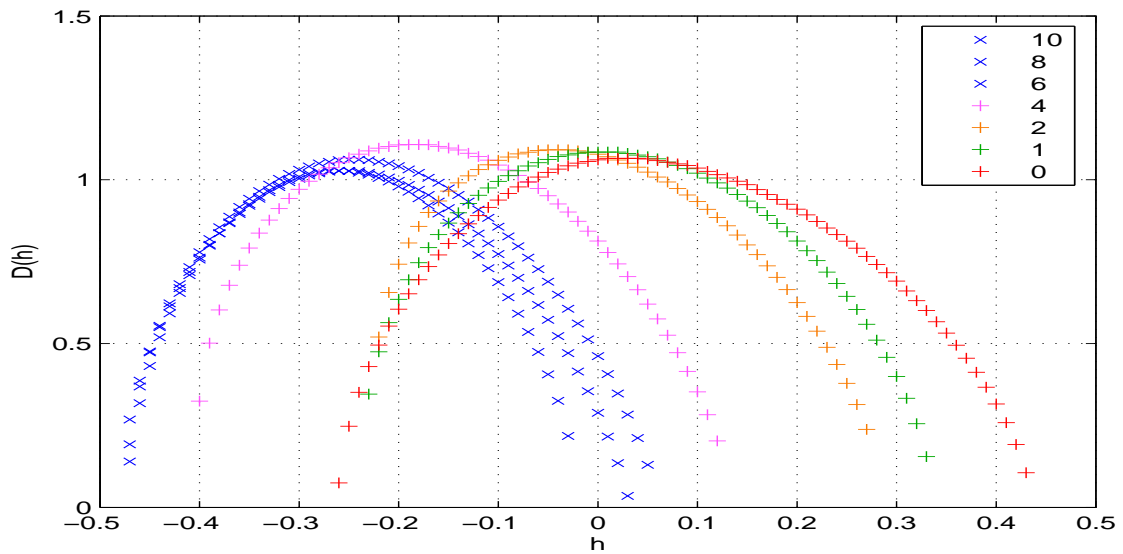


Figure 26: NAM index (100 hPa) + quadratic component: Singularity spectra for various derivatives of the Gaussian function as wavelet mother

component.

$$X_n = \rho X_{n-1} + \sqrt{1 - \rho^2} y_n. \tag{16}$$

with $|\rho| < 1$ and y_n a random number. Depending on the choice of the autocorrelation parameter ρ , we can create a family of noise from white noises with $\rho = 0$ to strong red noises with $\rho = 0.9$. First, we created a such family of noises of the same length as the NAM index for several values of ρ . Then we performed the same computations using 50 windows of size 1 year, 5 years and 25 years. For each period of time, we computed the mean value of h obtained for the 50 windows. The results obtained for these computations are summarized in Table 1. As can be easily observed from the results, the method gives a good description

ρ	0.1	0.3	0.5	0.7	0.9
1 year	-0.31	-0.24	-0.13	0.03	0.30
5 years	-0.42	-0.40	-0.38	-0.30	-0.06
25 years	-0.42	-0.44	-0.43	-0.42	-0.35

Table 1: Mean values of h ($\max D(h)$) for several red noises

of the artificially created red noises. When using a short window of size 1 year, the mean value of h goes from -0.31 for $\rho = 0.1$ to 0.30 for $\rho = 0.9$. As expected, this size of window is suitable for describing short-range correlated signals. The window of size 5 years is less adapted for this kind of correlation, and the larger window of size 25 years is completely blind to short-range correlation. These results show that the wavelet-based multifractal method presented in this paper is well adapted for studying this kind of correlations.

Now, we can use the data given in Table 1 to comment the numerical results obtained for the NAM index. Indeed, with a window of size 1 year, we found for the stratosphere mean values of h bigger or equal to 0.5. That corresponds to a correlation stronger than a red noise with $\rho = 0.9$ indicating that the stratosphere anomalies are not a simple red noise. For

the same period of time, we can observe that the troposphere anomalies present a behavior similar to a red noise with a autocorrelation parameter around 0.7. If we consider now the results obtained with a window of size 5 years, we can remark that the stratosphere anomalies present a correlation stronger than a simple red noise. For the troposphere, we obtain numerical results similar to a red noise. Even with a window of size 25 years, we can observe that the stratosphere anomalies present a correlation stronger than a regular red noise. This is particularly true for the values of h obtained at 100 hPa which are around -0.2 above the results obtained for the different red noises.

4 Conclusion

In this paper, we have discussed some issues relating to the estimation of the multifractal nature of atmospheric data using a wavelet-based method. Our study reveals the clear fractal pattern of the analyzed series and their different scaling characteristics. In the case of the stratosphere, we found a short-range correlation behavior that occurs for short ranges of time scales, from few days to few months. In the troposphere and in the same ranges of time, we found a much weaker correlation. These results show in particular that classical weather forecasting, mainly based on tropospheric data, are clearly unreliable for periods longer than 5 days. We also compared the results obtained for the NAM index to the results obtained for artificially created red noises. The stratosphere anomalies present clearly some correlations stronger than usual red noises. The correlations in the troposphere are weaker and often similar to a red noise. Furthermore, the fact that we obtained the same results for various wavelet mothers with different vanishing moments proves that the signals do not present any polynomial components.

The properties described in this paper motivate the use of multifractal models for analyzing atmospheric data and simulating weather phenomena. The connection of the multiscaling

properties of atmospheric data to the underlying physical dynamics falls beyond the scope of the present paper. But we can confirm that cascade models that include scaling space-time anisotropy, causality and continuous scales have to be used in order to get reliable predictions. We have shown that tropospheric data present behaviors similar to red noises. So models for weather forecasting have to include red noise type generators in order to take into consideration this property of tropospheric data.

By using a two dimensional wavelet transform, we plan to extend our research from time series to spatial patterns of atmosphere analysis.

Acknowledgments

The research was supported by the National Science Foundation, Climate Dynamics Program, under grant ATM-0332364, and the DGA (French Defense Department) under contract 06.60.018.00.470.75.01. The author would like to thank Prof. KK. Tung for many fruitful conversations.

References

- [1] Antoine, J.P., Barache, D., Cesar Jr, R.M., Costa L. da F. (1996), Multiscale shape analysis using the continuous wavelet transform, IEEE Proc. Intern. Conf. Image Proc., **1**, 291-294.
- [2] Arneodo, A., Grasseau, G., Holschneider, M. (1988), Wavelet transform of multifractals, Phys. Rev. Lett., bf 61, 2281-2284.
- [3] Arneodo, A., Bacry, E., Muzy, J.F. (1995), The thermodynamics of fractals revisited with wavelets, Physica A, **213**, 232-275.

- [4] Arneodo, A., Argoul, F., Bacry, E., Elezgaray, J., Muzy, J.F. (1995), *Ondelettes, multifractales et turbulence*, Diderot Editeur, Paris, France.
- [5] Bacry, E., Muzy, J.F., Arneodo, A. (1993), Singularity spectrum of fractals signal from wavelet analysis: Exact results, *J. Stat. Phys.*, **70**, 635-674.
- [6] Baldwin, M.P., Dunkerton, T.J. (2001), Stratospheric harbingers of anomalous weather regimes, *Science*, **294**, 581-584.
- [7] Baldwin, M.P., <http://www.nwra.com/resumes/baldwin/nam.php>
- [8] Camp C.D., Tung, K.K. (2007), The influence of the solar cycle and QBO on the late winter stratospheric polar vortex, *J. Atmos. Sci.*, **64**, 1267-1283.
- [9] Coughlin K., Tung, K.K. (2005), Empirical Mode Decomposition of Climate Variability in the Atmospheric, in *Hilbert-Huang Transform: Introduction and Applications*; edited by N. Huang and S. Shen; World Scientific Publishing.
- [10] Coughlin K., Tung, K.K. (2005), Tropospheric Wave Response to Descending Decelerations in the Stratosphere, *J. Geophys. Res.*, **110**, D01103, doi:10.1029/2004JD004661.
- [11] Frisch, U. (1995), *Turbulence: The legacy of A.N. Kolmogorov*, Cambridge Univ. Press, Cambridge.
- [12] Jaffard, S. (1997) Multifractal formalism for functions Part I: Results valid for all functions, *SIAM J. Math. Anal.*, **28**, 944-970.
- [13] Jaffard, S. (1997) Multifractal formalism for functions Part II: Self-similar functions, *SIAM J. Math. Anal.*, **28**, 971-998.
- [14] Julian, P.R., Labitzke, K. (1965) A study of atmospheric energetics during the January-February 1963 stratospheric warming, *J. Atmos. Sci.*, **22**, No. 6, 597-610.

- [15] Mallat, S., Zhong, S. (1991), Wavelet transform maxima and multiscale edges, in: R.M. B. et al. (Eds.), Wavelets and their Applications, Jones and Bartlett, Boston.
- [16] Mallat, S. (1998) A wavelet tour of signal processing, Academic Press, New York.
- [17] Mandelbrot B.B. (1977), Fractals: Form, chance and dimension, Freeman, San Francisco.
- [18] Mandelbrot B.B. (1982), The fractal geometry of nature, Freeman, New York.
- [19] Muzy, J.F., Bacry, E., Arneodo, A. (1991), Wavelets and multifractal formalism for singular signals: application to turbulence data, Phys. Rev. Lett., **67**,3515-3518.,
- [20] NOAA-CIRES Climate Diagnostics Center in Boulder, Colorado, USA,
<http://www.cdc.noaa.gov>
- [21] Parisi, G., Frisch, U. (1985), On the singularity structure of fully developed turbulence, in Turbulence and Predictability in Geophysical Fluid Dynamic, edited by Ghil M., Benzi R. and Parisi G., North-Holland, Amsterdam.
- [22] Quiroz, R.S. (1977) Tropospheric-stratospheric polar vortex breakdown of January 1977, Geophys. Res. Lett., **4**, 151-154.